A&A 489, 1175–1182 (2008)
DOI: 10.1051/0004-6361:200810556

Astronomy & Astrophysics

Detection of 6.7 GHz methanol absorption towards hot corinos

J. D. Pandian[1], S. Leurini[2], K. M. Menten[1], A. Belloche[1], and P. F. Goldsmith[3]

[1] Max-Planck-Institut für Radioastronomie, Auf dem Hügel 69, 53121 Bonn, Germany
e-mail: [jpandian;kmenten;belloche]@mpifr-bonn.mpg.de
[2] ESO, Karl-Schwarzschild Strasse 2, 85748 Garching-bei-München, Germany
e-mail: sleurini@eso.org
[3] Jet Propulsion Laboratory, Pasadena, CA 91109, USA
e-mail: Paul.F.Goldsmith@jpl.nasa.gov

Received 9 July 2008 / Accepted 4 August 2008

ABSTRACT

Context. Methanol masers at 6.7 GHz have been found exclusively towards high-mass star forming regions. Recently, some Class 0 protostars have been found to display conditions similar to what are found in hot cores that are associated with massive star formation. These hot corino sources have densities, gas temperatures, and methanol abundances that are adequate for exciting strong 6.7 GHz maser emission.
Aims. This raises the question of whether 6.7 GHz methanol masers can be found in both hot corinos and massive star forming regions, and if not, whether thermal methanol emission can be detected.
Methods. We searched for the 6.7 GHz methanol line towards five hot corino sources in the Perseus region using the Arecibo radio telescope. To constrain the excitation conditions of methanol, we observed thermal submillimeter lines of methanol in the NGC 1333-IRAS 4 region with the APEX telescope.
Results. We did not detect 6.7 GHz emission in any of the sources, but found absorption against the cosmic microwave background in NGC 1333-IRAS 4A and NGC 1333-IRAS 4B. Using a large velocity gradient analysis, we modeled the excitation of methanol over a wide range of physical parameters, and verify that the 6.7 GHz line is indeed strongly anti-inverted for densities lower than 10^6 cm^{-3}. We used the submillimeter observations of methanol to verify the predictions of our model for IRAS 4A by comparison with other CH_3OH transitions. Our results indicate that the methanol observations from the APEX and Arecibo telescopes are consistent with dense ($n \sim 10^6$ cm^{-3}), cold ($T \sim 15$–30 K) gas.
Conclusions. The lack of maser emission in hot corinos and low-mass protostellar objects in general may be due to densities that are much higher than the quenching density in the region where the radiation field is conducive to maser pumping.

Key words. masers – stars: low-mass, brown dwarfs

1. Introduction

The 5_1–6_0 A^+ line of methanol at 6.7 GHz is the strongest of Class II methanol masers. 6.7 GHz masers are unique compared to OH and H_2O masers in that they are associated exclusively with high-mass star forming regions. For example, targeted searches towards low-mass young stellar objects have not resulted in any detections of 6.7 GHz methanol masers (Minier et al. 2003; Bourke et al. 2005; Xu et al. 2008). Theoretical models suggest that the maser emission switches on at gas densities greater than $\sim 10^4$ cm^{-3} and methanol fractional abundance greater than $\sim 10^{-7}$, along with the requirement of a far-infrared radiation field to excite methanol to torsionally excited states as part of the pumping cycle (Sobolev et al. 1997; Cragg et al. 2002, 2005). These conditions are found in high-mass star forming regions where the far-infrared radiation field is generated by warm dust ($T_D \sim 100$–150 K), and high methanol abundances are achieved by evaporating the mantles of dust grains, either by the passage of a shock or through the radiation field of the massive young stellar object. The molecules released from the grains further trigger formation of more complex molecules in warm gas chemistry (e.g. Charnley et al. 1992).

Recently, there has been evidence of hot core chemistry in low-mass protostars. For example, complex molecules such as $HCOOCH_3$, HCOOH, and CH_3CN have been found in IRAS 16293–2422 (Cazaux et al. 2003) and NGC 1333-IRAS 4A (Bottinelli et al. 2004) along with high abundance of H_2O, CH_3OH, and H_2CO (Ceccarelli et al. 2000a,b; Schöier et al. 2002). The abundance of methanol in the compact, warm regions in the immediate proximity of these embedded sources, known as hot corinos, can be as high as 7×10^{-7} (Maret et al. 2005, and references therein). Moreover, the regions have warm temperatures (>100 K) and high densities (>10^7 cm^{-3}; Ceccarelli et al. 2000a). This raises the question of whether hot corinos can excite maser emission in Class II methanol lines. A discovery of Class II methanol masers in hot corinos would force re-interpretation of the methanol maser data in the literature. In this paper, we report on the results of a search for 6.7 GHz methanol masers towards five hot corino sources in the Perseus region.

2. Observations

2.1. Arecibo observations

The search for 6.7 GHz maser emission towards hot corinos was carried out using the 305 m Arecibo radio telescope[1] in

[1] The Arecibo Observatory is part of the National Astronomy and Ionosphere Center, which is operated by Cornell University under a cooperative agreement with the National Science Foundation.

Table 1. Hot corinos observed at 6.7 GHz. The columns show source name, equatorial J2000 coordinates and the rms noise in spectra.

Source	α (J2000)	δ (J2000)	S (rms) mJy
L1448–N.....	03 25 36.6	+30 45 15	1.2
L1448–MM.....	03 25 38.8	+30 44 05	1.3
NGC 1333–IRAS 2.....	03 28 55.4	+31 14 35	1.2
NGC 1333–IRAS 4A...	03 29 10.3	+31 13 31	1.0
NGC 1333–IRAS 4B...	03 29 12.0	+31 13 09	1.0

October 2006. The C-High receiver was used along with the "interim" correlator backend. Two units of the correlator were used with 1.5625 MHz bandwidth to measure two orthogonal linear polarizations with 9-level sampling and 1024 channels per polarization giving a velocity coverage of 140 km s^{-1} with 0.28 km s^{-1} resolution after Hanning smoothing. The adopted rest frequency for the transition was 6668.518 MHz; a more accurate measurement of 6668.519 MHz by Breckenridge & Kukolich (1995) gives an error of 0.04 km s^{-1} in the velocity scale, which is well below the resolution of the spectra. The sources observed and their coordinates are indicated in Table 1. Sources NGC 1333-IRAS 4A and NGC 1333-IRAS 4B had on-source integration times of 45 min each, while the remaining sources had on-source integration times of 30 min each. The data were taken in position switched mode. The "off" spectra were taken over the same elevation and azimuth range as for the "on" spectra to ensure cancellation of standing waves. During each observation, the pointing was checked using a continuum source and was found to be accurate within 10″. The system temperature was between 23 and 34 K, with approximately 20% difference between the two polarizations. The half-power beamwidth (*HPBW*) of the telescope at this frequency is ∼40″.

The data were reduced in IDL using procedures maintained by the observatory. The antenna temperature was derived using noise diodes, which was converted to flux density using an elevation and azimuth dependent gain curve for this frequency, the typical conversion factor being 5 K/Jy. The resulting rms noise in the spectra after Hanning smoothing was 1.0 mJy for IRAS 4A and IRAS 4B, and 1.2−1.3 mJy for the remaining sources. We did not carry out any baselining of the spectra.

2.2. APEX observations

It is possible to carry out an excitation analysis to reproduce the observed 6.7 GHz feature using millimeter and submillimeter lines of methanol (Leurini et al. 2004). In order to do this, we observed the NGC 1333-IRAS 4 region in the $(6_K - 5_K)$ CH_3OH band at ∼290 GHz using the APEX 12 m telescope[2]. The observations were carried out in November 2006 using the APEX2A double side band receiver (Risacher et al. 2006) and the Fast Fourier Transform Spectrometer (FFTS; Klein et al. 2006). The receiver was tuned to a frequency of 290.300 GHz in the lower sideband. One unit of the FFTS was centered at the tuning frequency, while the second unit was centered at 291.5 GHz. Both units had a bandwidth of 1 GHz with 16 384 channels, the effective velocity resolution being 0.13 km s^{-1} (since the noise in successive channels is correlated; Klein et al. 2006). The pointing was checked approximately every 1.5 h in CO (J = 3–2) on IK-Tau and was found to be accurate to within 2″. The focus was verified using Saturn. The system temperatures were typically 120−150 K in units of T_A^*. The half-power beamwidth of the telescope at this frequency is around 21″. A 1.5′ × 2.5′ region was mapped using the on-the-fly scanning mode with a step size of 6″.

The data were reduced using the CLASS software. A first order polynomial was fitted to the line-free channels and subtracted off the baseline. The data were converted to main beam temperature units (T_{MB}) assuming a beam efficiency of 0.73 and a forward efficiency of 0.97 (Güsten et al. 2006). Individual lines were then identified using the XCLASS software (Comito et al. 2005).

[2] This publication is based on data acquired with the Atacama Pathfinder Experiment (APEX). APEX is a collaboration between the Max-Planck-Institut für Radioastronomie, the European Southern Observatory, and the Onsala Space Observatory.

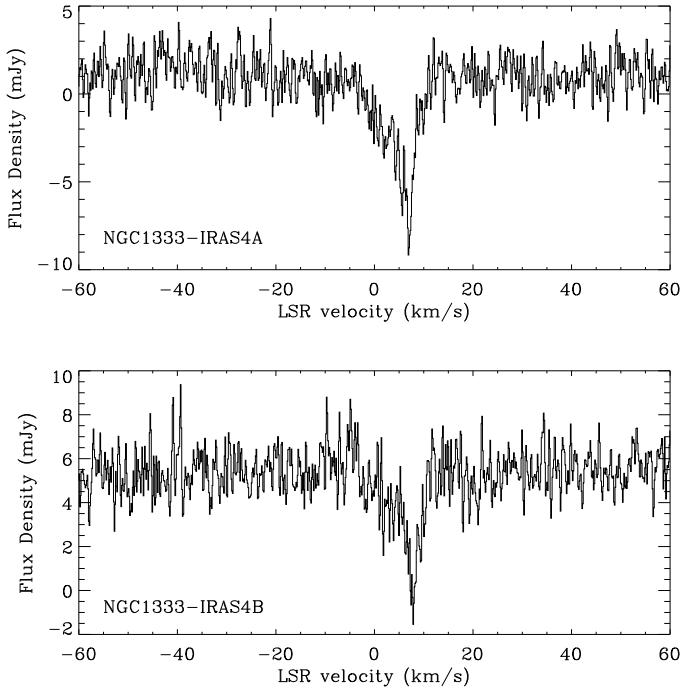

Fig. 1. The observed 6.7 GHz spectra showing absorption in NGC 1333-IRAS 4A and IRAS 4B.

3. Results

We did not detect 6.7 GHz maser emission in any of the sources, but detected prominent absorption in NGC 1333-IRAS 4A and NGC 1333-IRAS 4B, as shown in Fig. 1. IRAS 4A and IRAS 4B are separated by 31″, which is less than the half-power beamwidth of 40″. Thus, the measured spectrum towards IRAS 4A has some contribution from IRAS 4B and vice versa. Assuming a symmetric beam, if α is the contribution of the second source at the position of the first, then the measured spectra can be written as

$$S^{\rm m}_{\rm IRAS\ 4A} = S^{\rm a}_{\rm IRAS\ 4A} + \alpha S^{\rm a}_{\rm IRAS\ 4B} \quad (1)$$

$$S^{\rm m}_{\rm IRAS\ 4B} = S^{\rm a}_{\rm IRAS\ 4B} + \alpha S^{\rm a}_{\rm IRAS\ 4A} \quad (2)$$

where $S^{\rm a}$ and $S^{\rm m}$ indicate the actual and measured spectra respectively. Since the beam is a Gaussian to good approximation at 31″ from center, the parameter α is calculated as 0.19. Equations (1) and (2) can then be inverted to calculate the actual spectra, the results being shown in Fig. 2. The contribution of IRAS 4B to the observed IRAS 4A spectrum is small (less than ∼10%), while the contribution of IRAS 4A to the observed IRAS 4B spectrum is much more significant (∼30%).

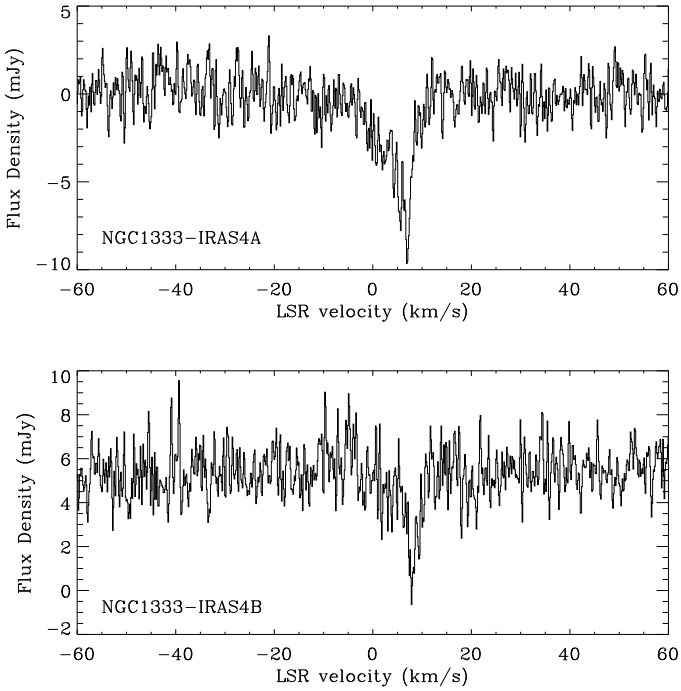

Fig. 2. 6.7 GHz spectra of NGC 1333-IRAS 4A and IRAS 4B that have been deconvolved to remove their mutual contamination. A comparison with Fig. 1 reveals that the spectrum of IRAS 4A is almost identical, while IRAS 4B shows a more significant difference.

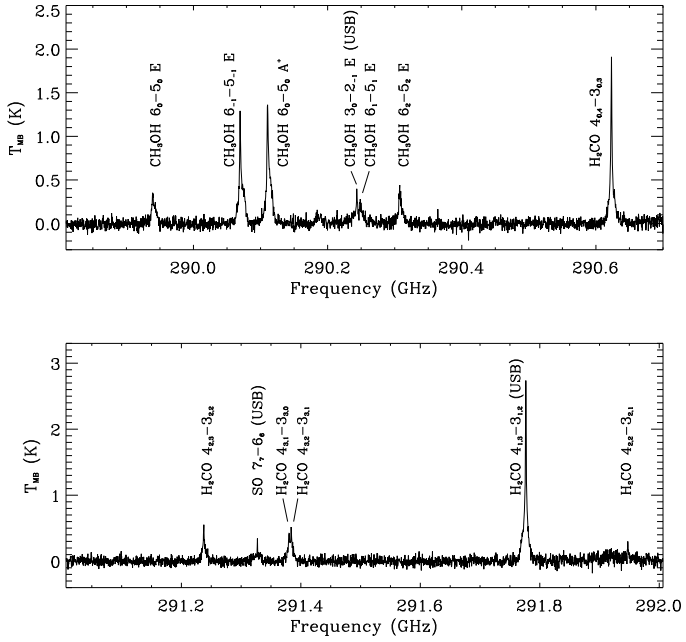

Fig. 3. APEX spectra of NGC 1333-IRAS 4A smoothed to the Arecibo resolution of 40″ (*HPBW*).

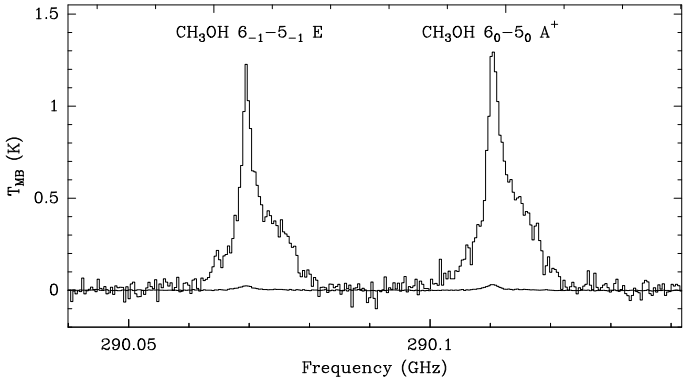

Fig. 4. The higher intensity spectrum shows two 290 GHz methanol lines from the APEX data towards IRAS 4A that is smoothed to 40″ resolution and includes contributions from IRAS 4B. The weaker spectrum represents the difference between that spectrum and another 40″ resolution spectrum from the same position that does not include data in the direction of IRAS 4B. The "contamination" from IRAS 4B is thus estimated to be at most 3.5%.

For modeling the observed 6.7 GHz absorption, we smoothed the APEX data to the spatial scale of the Arecibo beam. The resulting spectrum at the IRAS 4A position is shown in Fig. 3. We were unable to obtain spectra from the smoothed data cube at the IRAS 4B position since the footprint of the Arecibo beam at this location extends beyond the eastern edge of the APEX map. Since the convolution will give rise to the same degree of blending between the two sources as in the Arecibo observation, one would ideally have to deconvolve the spectra of the two sources extracted from the smoothed data cube, using the same parameters as for the Arecibo data. In the absence of spectra from both IRAS 4A and IRAS 4B at the same spatial resolution, it is not possible to deconvolve the two sources as was carried out for the Arecibo data. To quantify this contamination in the APEX data, we extracted a spectrum from IRAS 4A taking care to exclude the IRAS 4B region during the spatial convolution, and compared it with the spectrum at the same position from the original smoothed datacube (which includes the contribution from IRAS 4B). Figure 4 shows the difference between the two spectra overlaid on the IRAS 4A spectrum from the smoothed datacube. From this analysis, we estimate the contribution of IRAS 4B to IRAS 4A in the APEX data to be at most 3.5%. Henceforth, we will ignore the contamination of IRAS 4B on IRAS 4A. Since the contribution of IRAS 4A to the IRAS 4B spectrum is significant, we do not model IRAS 4B.

Figure 5 shows the 6.7 GHz absorption spectrum measured towards IRAS 4A and the 290.1 GHz thermal methanol emission over the same velocity range. The similarity of the line shapes of the two lines is striking. From the channel maps of the 290.1 GHz line (Fig. 6), it can be seen that the emission around 0 km s^{-1} and 11 km s^{-1} (LSR) arises from the blue and red-shifted lobes respectively of the outflow in IRAS 4A. In contrast, the continuum emission from the region at centimeter wavelengths is concentrated over a 0.42″ × 0.28″ region at the core (Reipurth et al. 2002). Moreover, the continuum flux density at 3.6 cm is 0.43 mJy (adding the emission from IRAS 4A1 and IRAS 4A2 components; Reipurth et al. 2002) which is more than an order of magnitude weaker than the observed depth of absorption (several orders of magnitude weaker when accounting for beam dilution). This indicates that the 6.7 GHz line is being absorbed against the cosmic microwave background (CMB) over the full spatial extent of thermal methanol emission (including the outflow), as opposed to absorption against the continuum from the core. This is similar to the observation of 12.2 GHz absorption against the CMB in dark clouds by Walmsley et al. (1988).

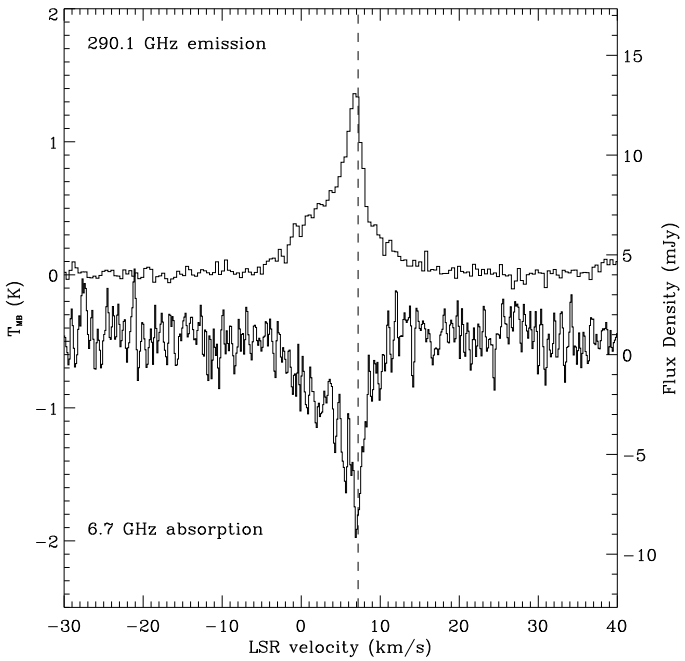

Fig. 5. A comparison of the line profiles of 290.1 GHz emission (*left axis*) and 6.7 GHz absorption (*right axis*) of methanol in NGC 1333-IRAS 4A. The location of peak emission/absorption is indicated by the dashed line. The similarity of the line profiles indicates that the 6.7 GHz line is being absorbed over the full spatial extent of thermal methanol emission.

4. Statistical equilibrium calculations

4.1. Anti-inversion in the 5_1-6_0 A^+ 6.7 GHz transition

As first realized by Batrla et al. (1987), methanol masers come in two varieties, termed Class I and II by Menten (1991a,b). Class II methanol masers are closely associated with young high-mass (proto)stellar objects and arise from the same regions as hydroxyl (OH) masers. Like OH masers, Class II methanol masers are most likely pumped by far-infrared radiation in dense ($n \sim 10^7$ cm^{-3}), warm ($T \sim 150$ K) gas (Cesaroni & Walmsley 1991; Cragg et al. 2002; Sobolev & Deguchi 1994a,b; Sobolev et al. 1997). In contrast, Class I methanol masers are frequently found in the general vicinity of intermediate and high-mass star formation, but often significantly offset (up to a parsec) from prominent center of activity, such as infrared sources or compact radio sources (e.g., Menten et al. 1986). Moreover, their pumping mechanism can be explained from basic properties of the methanol molecule (Lees 1973; Lees & Haque 1974). Often, Class I methanol masers are accompanied by absorption in the Class II maser lines against either the CMB (e.g., Walmsley et al. 1988; Whiteoak & Peng 1989) or the continuum of the source (Whiteoak et al. 1988; Menten 1991b; Peng & Whiteoak 1992). The excitation properties of the 12.2 GHz line in absence of a strong infrared radiation field were explained in detail by Walmsley et al. (1988). The 6.7 GHz line was predicted to be anti-inverted (i.e. over-cooled) under conditions similar to those producing anti-inversion in the 12.2 GHz line by Menten (1991b) and Cragg et al. (1992). To our knowledge, the 6.7 GHz line has been detected in absorption mostly against the radio continuum of the source (e.g., Menten 1991b; Impellizzeri et al. 2008), and the only detections of absorption against the CMB are what is reported here, and probably, in the star forming region NGC 2264 (Menten 1991b).

To investigate the physical conditions leading to absorption of the 6.7 GHz line against the CMB, we carried out a large velocity gradient (LVG) analysis with spherical geometry (Leurini et al. 2004, 2007). In contrast to the approach used by Leurini et al. (2007) for modeling high-mass star forming regions, the only external radiation field used in our calculations is that of the CMB. Moreover, only a sub-sample of energy levels (the first 100 levels) was used for the calculations.

Figure 7 shows the results of our calculations for the 5_1-6_0 A^+ transition at 6.7 GHz, for two different CH_3OH-*A* column densities (10^{14} and 10^{16} cm^{-2}), at temperatures of 10, 30 and 50 K. A linewidth of 1 km s^{-1} was assumed for all cases. For comparison, the 2_0-3_{-1}-*E* line at 12.2 GHz is also shown. It can be seen that both lines have a very similar behavior. They are strongly anti-inverted at low densities ($n \leq 10^6$ cm^{-3}) in absence of an infrared radiation field, the primary difference being that the 6.7 GHz line is quenched at higher densities compared to the 12.2 GHz line. For both lines, the intensity of absorption increases with abundance of CH_3OH. Moreover, the density at which the absorption line intensity is maximum, decreases with increasing temperature. Since the only radiation field in our calculations is that of the CMB, our results are not applicable for sources that have an IR radiation field, whose effect among others is to produce strong masers in both lines. For a discussion of the excitation of the 6.7 and 12.2 GHz in the presence of IR radiation fields, we refer to Sobolev & Deguchi (1994b) and Sobolev et al. (1997), or to the more recent work of Cragg et al. (2005).

We can verify the predictions of our analysis by simultaneously modeling the CH_3OH spectrum at 6.7 GHz and 290 GHz, assuming that the lines at the two wavelengths trace the same gas. In the next section, we will model the CH_3OH emission of NGC 1333-IRAS 4A. As discussed in Sect. 3, we refrain from a similar analysis for IRAS 4B, as the source lies near the edge of the area mapped with APEX, preventing us from obtaining a spectrum of the source at the spatial resolution of the Arecibo data.

4.2. Methanol around IRAS 4A

As explained in Sect. 3, to model the two datasets, we smoothed the 290 GHz spectrum to the spatial resolution of the 6.7 GHz observations (*HPBW* of 40″). The similarity of the line profiles at 6.7 GHz and 290 GHz (Fig. 5) strongly suggests that the absorption at 6.7 GHz arises from the same gas that gives rise to 290 GHz emission. Hence, to interpret the APEX and Arecibo CH_3OH data, we applied the method described by Leurini et al. (2004), based on an LVG analysis and simultaneous fitting of the entire spectrum with different non-interacting velocity components, each of them being characterized by its source size, kinetic temperature, column density and density.

The interpretation of our observations is rendered difficult by the complexity of the IRAS 4 region and by the poor spatial resolution of our data. The 40″ Arecibo beam includes the hot corino IRAS 4A, and the molecular outflow originating from it (Choi 2001, 2005). As discussed in Sect. 3, contamination from IRAS 4B at this position is small enough to be neglected.

The line profiles are characterized by strong blue-shifted and weaker red-shifted emission. The same asymmetry between the blue- and red-shifted emission that can be seen in our CH_3OH data was observed by Belloche et al. (2006) in CS. From the channel maps at 21.7″ resolution of the CH_3OH (6_K-5_K) band (Fig. 6), we conclude that the blue-shifted and red-shifted emission come from compact sources to the north and south of IRAS 4A respectively. By fitting the peak of

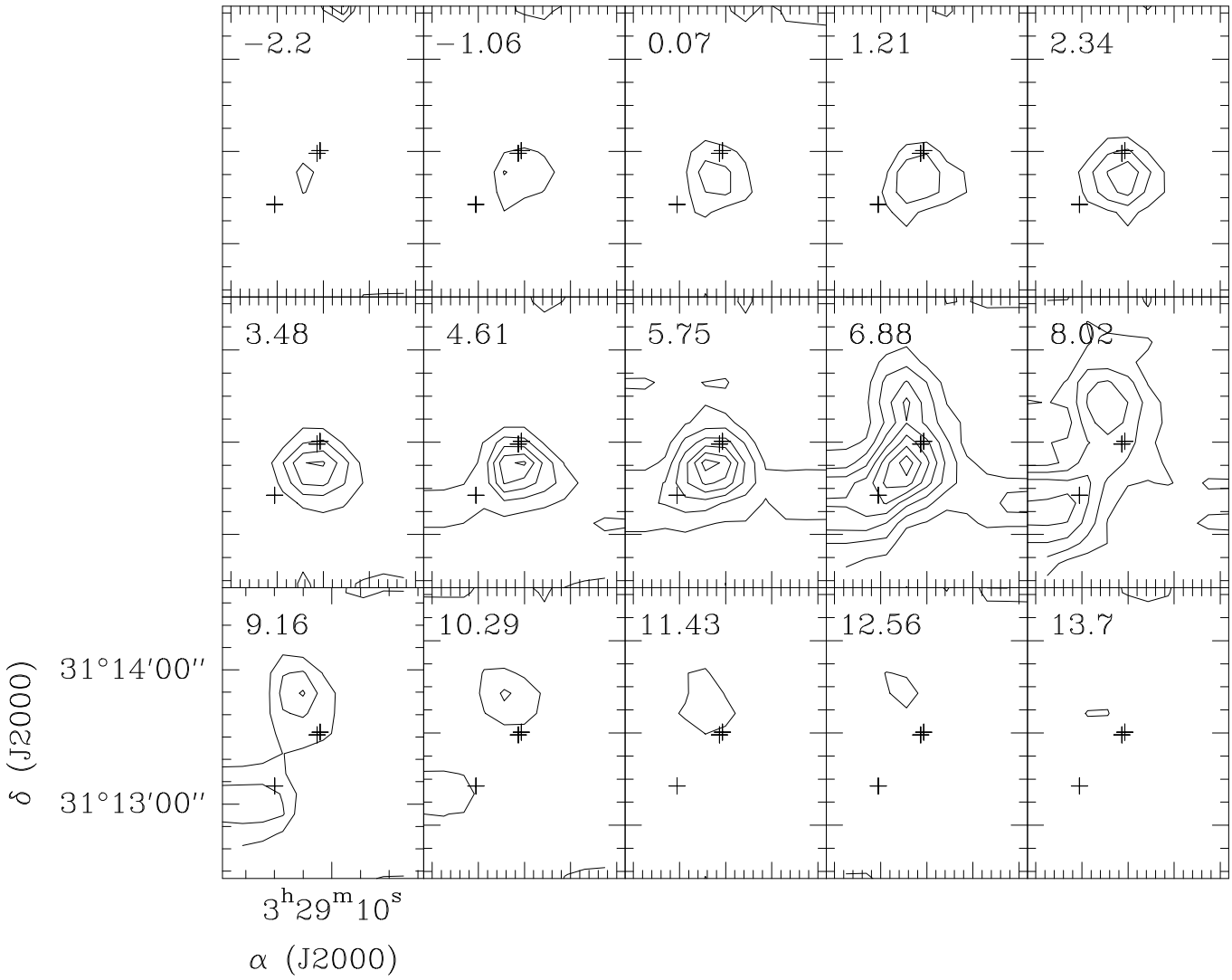

Fig. 6. Channel maps of the CH_3OH 6_0-5_0 transition at 290.11 GHz obtained with APEX and smoothed to a spectral resolution of 1.1 km s^{-1}. The channel velocity is written in *the top left corner* of each panel. The crosses mark the positions of the protostars IRAS 4A1, 4A2, and 4B (Looney et al. 2000). The emission below 4 km s^{-1} and above 11 km s^{-1} is associated with the bipolar outflow powered by IRAS 4A. The contour levels are at integer multiples of 0.25 K.

the integrated intensity map of the blue-shifted wing of the 6_0-5_0-A^+ line at 290.1 GHz (in the range of −2.5 to 4 km s^{-1}) with a two dimensional elliptical Gaussian and deconvolving for the APEX beam, we estimate a source size of 14″ for the blue lobe. A similar source size is obtained for the red lobe, using the integrated emission of the red-shifted wing of the H_2CO ($4_{0,4}-3_{0,3}$) line, which is stronger than the CH_3OH (6_K-5_K) transitions. However, the signal to noise ratio in the red wing is lower than that of the blue wing, resulting in higher uncertainties. Emission around the central velocity is centered close to IRAS 4A, but is elongated along the north-south direction and is probably contaminated by the blue and red lobes. This is also seen in the CH_3OH ($6_{\pm2}-5_{\pm2}$)-E lines, which are too weak for a channel map analysis, but whose integrated intensity map shows three peaks, corresponding to IRAS 4B, and the blue and red lobes of the molecular outflow from IRAS 4A. However, the peak corresponding to the blue lobe of the outflow extends to the core of IRAS 4A.

We modeled the spectrum using three velocity components, each having a compact size of 14″, corresponding to the blue- and red-shifted emission and the hot corino in IRAS 4A. Since the red lobe emission is detected in fewer transitions, we mostly use this component more to obtain a reasonable fit of the line profiles than to derive its physical conditions. Figure 8 shows the best fit model spectrum for the 6.7 GHz line and the (6_K-5_K) band, overlaid on the observed spectra. The best fit parameters are: T = 17 K, n = 2 × 10^6 cm^{-3}, and $N(CH_3OH)$ = 4 × 10^{15} cm^{-2} for the core velocity component; T = 27 K, n = 4 × 10^6 cm^{-3}, $N(CH_3OH)$ = 2 × 10^{15} cm^{-2} for the blue-shifted component; and T = 29 K, n = 1 × 10^6 cm^{-3}, $N(CH_3OH)$ = 10^{15} cm^{-2} for the red-shifted component. The linewidths used in the model are 1.9, 7 and 8 km s^{-1} for the core, blue-shifted and red-shifted components, respectively.The total column densities are derived assuming the same abundance for the two symmetry states, A and E.

The 290 GHz observations include the 3_0-2_{-1} E line of methanol at 302.369 GHz from the upper sideband of the APEX-2A receiver. However, since the sideband ratio of the receiver as a function of frequency is not well known, we did not include this line in our calculations. We did compare the line intensity predicted by the best fit model with the intensity in our data. The model predicts a line intensity T_{MB} ∼ 0.6 K against the

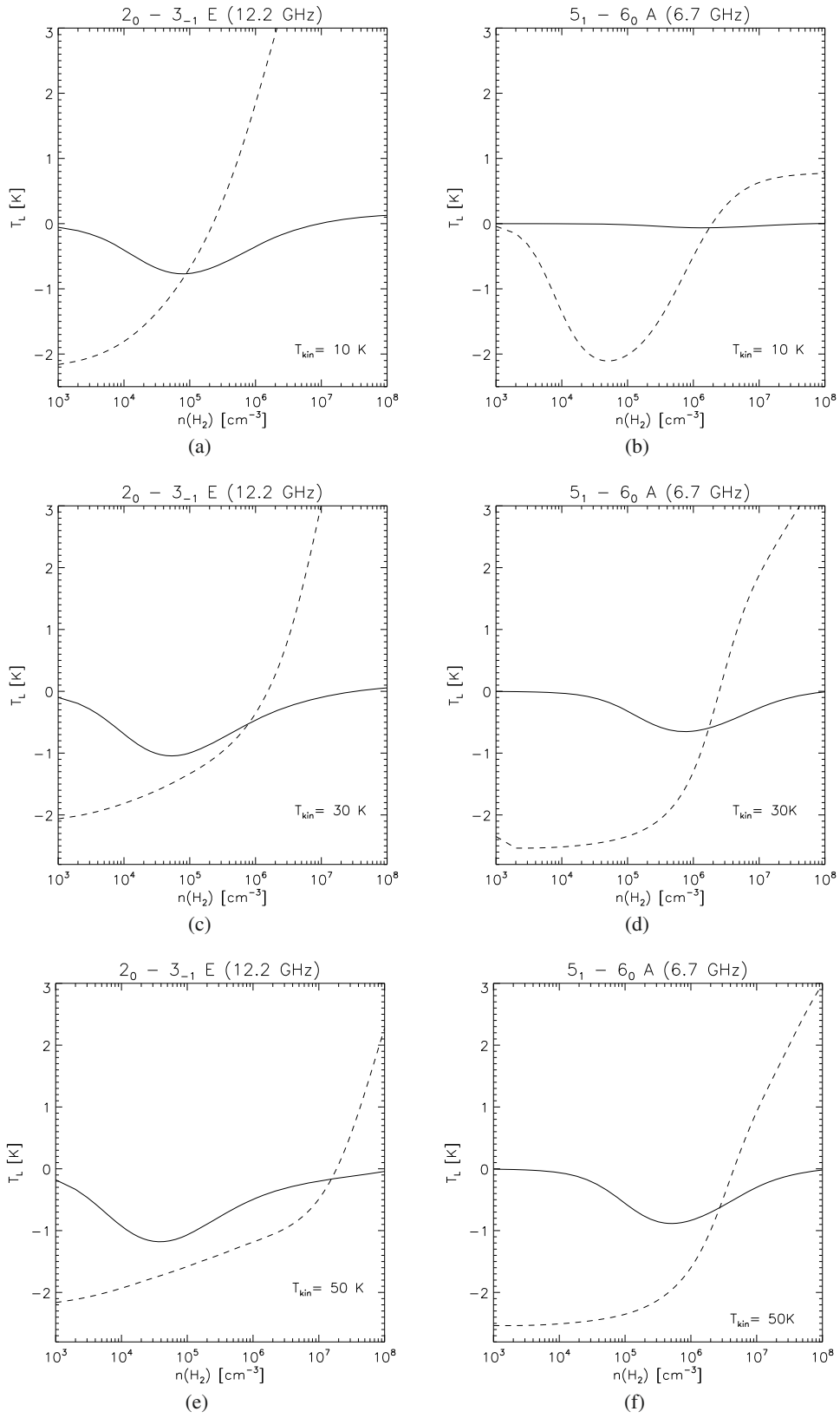

Fig. 7. Results of statistical equilibrium calculations for the 2_0-3_{-1}-*E* (*left column*) and 5_1-6_0-A^+ (*right column*) transitions. The solid and dashed lines show the predicted line intensities for CH_3OH column densities (for both *E* and *A* species) of 10^{14} cm^{-2} and 10^{16} cm^{-2} respectively, and a linewidth of 1 km s^{-1}.

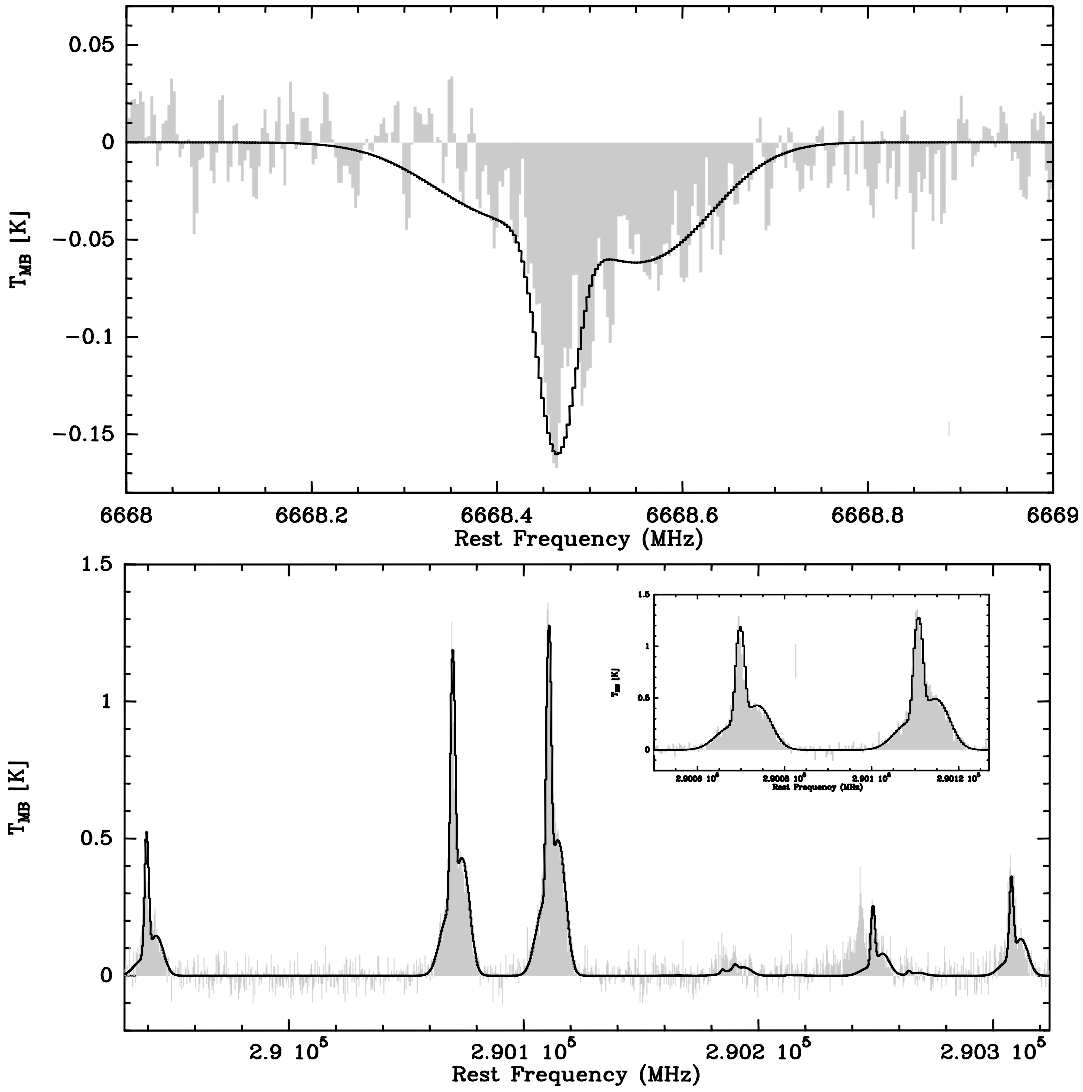

(a)

Fig. 8. Methanol spectra at 6.7 GHz (*top*) and 290 GHz (*bottom*) towards NGC 1333-IRAS 4A. The solid line represents the synthetic spectrum for the best fit parameters. The inset in *the bottom panel* shows the $6_{-1}-5_{-1}$-E and 6_0-5_0-A^+ lines in greater detail.

observed value of 0.2 K. Since the sideband ratio of the receiver at this frequency is not known, and since no other solution that fit all lines was found, we believe our results to be compatible with the data.

We refrain from a more rigorous analysis of our results due to the complexity of the region, coarse resolution of the data, and the limited number of transitions available for modeling. Our observations are mostly sensitive to the density of the gas and the CH_3OH column density. However, since the emission is optically thin, similar results can be achieved by increasing the column density of one of the components and decreasing its corresponding source size and vice versa. Finally, the low temperature derived by our analysis is mostly constrained by the weakness of the 6.7 GHz absorption. Although the fit is not excellent (with a reduced χ^2 of 2), the model predictions for the 6.7 GHz absorption are compatible with our observations at 290 GHz.

4.3. Why do we not observe class II methanol maser emission?

According to Cragg et al. (2005) the 6.7 GHz CH_3OH line shows strong maser action for dust temperatures, T_D, above 120 K. To estimate the radius, r_{120}, of the region around IRAS 4A within which that value is attained, we use the Stefan-Boltzmann law, since the dust emission is certainly optically thick at all relevant wavelengths. We assume a bolometric luminosity, L_*, of 11.6 $L_\odot$, where we have scaled the estimate of Sandell et al. (1991) to the Hipparcos distance of the Per OB2 association, i.e., 318 pc (de Zeeuw et al. 1999). We calculate r_{120} to be 37 AU. Optically thin dust emission, e.g. with an emissivity index, β, of 0.85, derived by Belloche et al. (2006, see their Eq. (1)), would yield an even smaller r_{120} of 22 AU. Modeling IRAS 4A's circumstellar environment as a collapsing envelope, Belloche et al. (2006) derive relations between the density, n, and radial distance, r, for $r > 500$ AU at different times. At $r = 500$ AU, their "best fit" model predicts a density of $n = 10^7$ cm^{-3} and their data suggests a density that may even be a factor of 3 greater. While extrapolating the density to r_{120} (37 AU) may not be straightforward, it is almost certain that the density that close to the central object will be vastly in excess of the 10^8 cm^{-3} at which any maser action would be quenched (see Fig. 3 of Cragg et al. 2005).

This realization may be extended to low-mass protostars/hot corinos in general and explains the notorious absence of class II

methanol masers around such objects (see, a.o, the extensive survey of Minier et al. 2003). In plain words: for low-mass protostellar objects, the region in which the radiation field would allow maser pumping is so dense that the maser emission is quenched, i.e., the 6.7 GHz transition's energy levels are thermalized.

5. Conclusions

We have made the first conclusive detection of absorption of the 6.7 GHz line against the CMB towards hot corino sources NGC 1333-IRAS 4A and NGC 1333-IRAS 4B. A LVG analysis indicates that the 6.7 GHz line is indeed strongly anti-inverted for densities lower than 10^6 cm^{-3} almost independent of temperature. Using observations of submillimeter 6_K–5_K lines of methanol using the APEX telescope, we model NGC 1333-IRAS 4A, and are able to reproduce the observed 6.7 GHz absorption using cold ($T \sim 15$–30 K), dense ($n \sim 10^6$ cm^{-3}) gas. The absence of maser emission at 6.7 GHz in hot corinos, and low-mass protostellar objects in general, is presumably due to the very high densities in the region where the radiation field would provide for maser pumping.

Acknowledgements. This work was supported in part by the Jet Propulsion Laboratory, California Institute of Technology, under a contract with the National Aeronautics and Space Administration. This research has made use of NASA's Astrophysics Data System.

References

Batrla, W., Matthews, H. E., Menten, K. M., & Walmsley, C. M. 1987, Nature, 326, 49
Belloche, A., Hennebelle, P., & André, P. 2006, A&A, 453, 145
Bottinelli, S., Ceccarelli, C., Lefloch, B., et al. 2004, ApJ, 615, 354
Bourke, T. L., Hyland, A. R., & Robinson, G. 2005, ApJ, 625, 883
Breckenridge, S. M., & Kukolich, S. G. 1995, ApJ, 438, 504
Cazaux, S., Tielens, A. G. G. M., Ceccarelli, C., et al. 2003, ApJ, 593, L51
Ceccarelli, C., Castets, A., Caux, E., et al. 2000a, A&A, 355, 1129
Ceccarelli, C., Loinard, L., Castets, A., Tielens, A. G. G. M., & Caux, E. 2000b, A&A, 357, L9
Cesaroni, R., & Walmsley, C. M. 1991, A&A, 241, 537
Charnley, S. B., Tielens, A. G. G. M., & Millar, T. J. 1992, ApJ, 399, L71
Choi, M. 2001, ApJ, 553, 219
Choi, M. 2005, ApJ, 630, 976
Comito, C., Schilke, P., Phillips, T. G., et al. 2005, ApJS, 156, 127
Cragg, D. M., Johns, K. P., Godfrey, P. D., & Brown, R. D. 1992, MNRAS, 259, 203
Cragg, D. M., Sobolev, A. M., & Godfrey, P. D. 2002, MNRAS, 331, 521
Cragg, D. M., Sobolev, A. M., & Godfrey, P. D. 2005, MNRAS, 360, 533
de Zeeuw, P. T., Hoogerwerf, R., de Bruijne, J. H. J., Brown, A. G. A., & Blaauw, A. 1999, AJ, 117, 354
Güsten, R., Nyman, L. Å., Schilke, P., et al. 2006, A&A, 454, L13
Impellizzeri, C. M. V., Henkel, C., Roy, A. L., & Menten, K. M. 2008, A&A, 484, L43
Klein, B., Philipp, S. D., Krämer, I., et al. 2006, A&A, 454, L29
Lees, R. M. 1973, ApJ, 184, 763
Lees, R. M., & Haque, S. 1974, Canadian J. Phys., 52, 2250
Leurini, S., Schilke, P., Menten, K. M., et al. 2004, A&A, 422, 573
Leurini, S., Schilke, P., Wyrowski, F., & Menten, K. M. 2007, A&A, 466, 215
Looney, L. W., Mundy, L. G., & Welch, W. J. 2000, ApJ, 529, 477
Maret, S., Ceccarelli, C., Tielens, A. G. G. M., et al. 2005, A&A, 442, 527
Menten, K. 1991a, in Atoms, Ions and Molecules: New Results in Spectral Line Astrophysics, ASP Conf. Ser., 16, 119
Menten, K. M. 1991b, ApJ, 380, L75
Menten, K. M., Walmsley, C. M., Henkel, C., & Wilson, T. L. 1986, A&A, 157, 318
Minier, V., Ellingsen, S. P., Norris, R. P., & Booth, R. S. 2003, A&A, 403, 1095
Peng, R. S., & Whiteoak, J. B. 1992, MNRAS, 254, 301
Reipurth, B., Rodríguez, L. F., Anglada, G., & Bally, J. 2002, AJ, 124, 1045
Risacher, C., Vassilev, V., Monje, R., et al. 2006, A&A, 454, L17
Sandell, G., Aspin, C., Duncan, W. D., Russell, A. P. G., & Robson, E. I. 1991, ApJ, 376, L17
Schöier, F. L., Jørgensen, J. K., van Dishoeck, E. F., & Blake, G. A. 2002, A&A, 390, 1001
Sobolev, A. M., & Deguchi, S. 1994a, ApJ, 433, 719
Sobolev, A. M., & Deguchi, S. 1994b, A&A, 291, 569
Sobolev, A. M., Cragg, D. M., & Godfrey, P. D. 1997, A&A, 324, 211
Walmsley, C. M., Menten, K. M., Batrla, W., & Matthews, H. E. 1988, A&A, 197, 271
Whiteoak, J. B., & Peng, R.-S. 1989, MNRAS, 239, 677
Whiteoak, J. B., Gardner, F. F., Caswell, J. L., et al. 1988, MNRAS, 235, 655
Xu, Y., Li, J. J., Hachisuka, K., et al. 2008, A&A, 485, 729